Journal of Applied Polymer Science

Effect of crosslinking procedure on structural, thermal, and functional performances of cellulosic nanofibers: A comparison between chemical and photochemical crosslinking

Sajedeh Khorshidi,[1] Atefeh Solouk,[1] Akbar Karkhaneh,[1] Hamid Mirzadeh,[2] Shahriar Sharifi,[3] Saeedeh Mazinani[4]

[1]Biomedical Engineering Faculty, Amirkabir University of Technology (Tehran Polytechnic), Tehran, Iran
[2]Polymer Engineering Faculty, Amirkabir University of Technology (Tehran Polytechnic), Tehran, Iran
[3]Department of Biomaterials Science and Technology, University of Twente, Enschede, The Netherlands
[4]Amirkabir Nanotechnology Research Institute (ANTRI), Amirkabir University of Technology, Tehran, Iran
Correspondence to: A. Solouk (E-mail: Atefeh.Solouk@aut.ac.ir) and S. Mazinani (E-mail: s.mazinani@aut.ac.ir)

ABSTRACT: In the current study, hydroxyethyl cellulose (HEC) based nanofibers were fabricated through electrospinning and then made water insoluble by chemical and photochemical crosslinking. Structural, thermal, and functional performances of electrospun fibers before and after crosslinking were fully assessed by a numerous techniques including microscopy, porosimetry, mechanical analysis, and cell culture study. Both crosslinking procures were found to able to preserve fibrous structure in an aqueous environment for short times, however; chemical process conferred better long-term morphological stability and cell compatibility. These findings suggest that chemically crosslinked HEC mats may perform as a promising electrospun tissue engineering scaffold. © 2016 Wiley Periodicals, Inc. J. Appl. Polym. Sci. **2016**, *133*, 43832.

KEYWORDS: crosslinking; electrospinning; fibers; polysaccharides

Received 30 November 2015; accepted 20 April 2016
DOI: 10.1002/app.43832

INTRODUCTION

Polysaccharides-based electrospun fibers have gained enormous interest in the tissue engineering scaffolds.[1] However, these fibers are mostly susceptible to dissolution once contacting aqueous media. Water instability and considerable loss of mechanical strength necessitate crosslinking procedures during or after spinning process.[2] Crosslinking can be performed either by heat, radiation, or chemical agents. Various crosslinking procedures induce different levels of water stability and impact scaffold properties.[3] In some cases, crosslinking pose unwanted structural or functional effects on final scaffold.[4,5]

Chemical crosslinking, which is based on using small molecules containing reactive groups capable of forming covalent bonds with polymer functional sites, suffers from the potential cytotoxicity of the residual crosslinkers and its side-effects on biocompatibility should be always considered.[2] When using photocrosslinking, there is always the possibility of either polymer chain scission or crosslinking. Moreover, the biocompatibility of the photo-initiator is a major concern. Cell tolerance has been observed using a few photo-initiators. In addition, the radical formed by light exposure may leach out over time and compromise.[6] Therefore, it is imperative to assess the impact of crosslinking approach on scaffold features and to choose a proper crosslinking route with least undesirable effects.

Our intension in this research was to make electrospun scaffolds from a biocompatible polymer with chemical structure similar to glycosaminoglycans (GAGs). So we have chosen hydroxyethyl cellulose (HEC) for our studies. HEC is a non-ionic hydrophilic natural polysaccharide with (1 → 4) glycosidic linkage representing the fine resemblance of GAGs of innate extra cellular matrix (ECM).[7,8] HEC is one of the derivates of cellulose endowed with water solubility and biodegradation in addition to native merits of cellulosic materials. However, HEC alone is not amenable to electrospinning. HEC blending with polyvinyl alcohol (PVA), a hydrophilic linear flexible polymer, not only facilitates the HEC processing but also forms a composite retaining mechanical strength and durability of PVA and the biological functionality of HEC.[9] Electrospinning of HEC using PVA as career is recently reported.[7,8,10,11] However, the effect of different crosslinking procedures on structural and functional

Additional Supporting Information may be found in the online version of this article.

Table I. Prepared Samples and Their Corresponding Labels

Sample description	As spun	GA crosslinked	Photocrosslinked
HEC/PVA mat with blend ratio of 36:64	HEC/PVA1	GC HEC/PVA1	PC HEC/PVA1
HEC/PVA mat with blend ratio of 45:55	HEC/PVA2	GC HEC/PVA2	
HEC/PVA mat with blend ratio of 54:46	HEC/PVA3	GC HEC/PVA3	

properties of HEC based fibers is still unexplained. Herein, to improve the mechanical properties and stabilities of electrospun HEC-based mats, the fibers were crosslinked through either chemical or photochemical reactions and the impacts of those methods on mat attributes were analyzed.

EXPERIMENTAL

Materials

HEC ($M_w = 300{,}000$) was purchased from Kelong Chemical Co. PVA ($M_w = 89{,}000$–$98{,}000$, 99% hydrolyzed), glutaraldehyde (GA), propanol, absolute ethanol, and phosphate buffered saline (PBS) tablets were all supplied from Sigma Aldrich.

Scaffold Fabrication

HEC/PVA electrospun scaffolds were fabricated as follows: briefly, 4% (wt/vol) solution of HEC and 12% (wt/vol) solution of PVA were prepared and blended in 36:64, 45:55, and 54:46 mass ratios. Three most effective parameters (i.e., blend ratios, flow rate, and collector speed) have been selected following parameters optimization using central composite design (CCD) of experiment design software (Design-Expert 8.0). The lowest and highest amount which was obtained experimentally was given to the software and other 3 points were selected by software. The blend solutions were magnetically stirred at room temperature for over 8 h, and then delivered through a 20-G blunt needle at a constant flow rate of 1 mL/h. The needle was positioned 18 cm from a grounded and aluminum foil covered collector. The spinning voltage was set at 30 kV, and the rotation rate was ~700 rpm. Electrospun scaffold with 36:64, 45:55, and 54:46 mass ratios were labeled as HEC/PVA1, HEC/PVA2, and HEC/PVA3, respectively.

Scaffold Crosslinking

The electrospun scaffolds were crosslinked via two different methods, i.e., chemical and photochemical procedures. For the chemical crosslinking, GA as vapor and solution was examined. For the former, the electrospun samples were kept in a vacuum desiccator saturated with 2% (vol/vol) aqueous GA solution. For the later, the fibrous membranes were impressed in a solution comprising propanol/water 95:5, 0.01 *M* HCl and 2% (vol/vol) GA for 16 h. The sample were then taken away and dried in a vacuum oven at 50 °C, and unreacted GA was neutralized by immersion into 0.2 *M* glycine solution overnight. The scaffold were then washed thoroughly in PBS and dried. Crosslinked samples with 36:64, 45:55, and 54:46 mass ratios were labeled as GC HEC/PVA1, GC HEC/PVA2, and GC HEC/PVA3, respectively.

Photochemical crosslinking necessitated some modifications in electrospinning procedure. Sodium benzoate with 1% (wt/wt) was added to electrospinning solution as a photoinitiator, and the UV lamp with 254 wave length ($\lambda = 254$ nm) and 15 W output power was placed parallel to with 10 cm distance from the collector. The UV lamp was then turned on and concurrent electrospinning and crosslinking was performed. Sample with blend ratio of 36:64 was selected for photochemical crosslinking and coded as PC HEC/PVA1. The samples and their corresponding codes are represented in Table I.

Solution Characterization

The viscosity was determined using a brookfield viscometer (RVDLII + Pro, Brookfield, USA) with a sample volume of 2 mL at a constant temperature of 26 °C. The conductivity was measured using a conductivity meter (Cond 7110, Cole-parmer, USA) with a sample volume of 10 mL at room temperature. All measurements were repeated three times.

Scaffold Characterization

Morphological Characterization. Morphology of the electrospun scaffolds was tested using scanning electron microscopy (SEM; AIS2100, Seron Technology, Korea) at an accelerating voltage of 20 kV after being sputter coated with Au particles. The fiber diameters were measured using image processing software (Image- Pro Plus 8.0) and the results are presented as average ± standard deviation calculated from sixty random measurements per image.

Porosimetry. Scaffold porosity in two steps (i.e., as electrospun, crosslinked electrospun scaffolds) was measured via two different methods named as gravimetry and liquid intrusion procedure. For the former, the scaffolds were cut into rectangular forms ($n = 4$), and the porosity estimated as $P(\%) = (1 - \rho_{ab}/\rho_s) \times 100$. Where ρ_{ab} is apparent density of the scaffolds, calculated as mass to volume ratio and ρ_s is the density of the scaffolds measured based on the weight ratio and respective densities of HEC ($\rho = 0.976$ g cm^{-3}) and PVA ($=1.190$ g cm^{-3}) in each sample. For the later, the rectangular dry specimens were weighed, submerge in absolute ethanol as an intruding liquid, left overnight on a shaker incubator to allow ethanol flow into the void spaces, wipe with tissue paper, and weighed again immediately. Thereafter, the porosity was calculated as $P\% = \frac{V_{EtOH}}{V_{EtOH} + V_s} \times 100$. where V_{EtOH} (the ratio between mass change after liquid intrusion and ethanol density) and V_s (scaffold mass to density ratio), refer to intruded ethanol and scaffold volume, respectively.[12,13] Pore diameters of electrospun scaffolds were also quantified from SEM micrographs using ImageJ. The diameters of the longest axes in 30 pores for each image were measured.

Fourier Transform Infrared Spectroscopy Characterization. Fourier transform infrared (FTIR) analysis of electrospun mats before and after crosslinking was performed using a FTIR (Bruker Equinox 55) in the range between 4000 and 400 cm^{-1}, with a resolution of 0.5 cm^{-1}. The specimens were examined on KBr disks at room temperature.

Tensile Testing. Tensile properties of the electrospun mats were measured using a uniaxial tensile testing machine with a 50 N load cell (TM–SM, Instron, England) at a constant strain rate of 1 mm/min until failure. Prior to testing, strip-shaped specimens (3 cm × 0.5 cm) were prepared, and the thickness of each strip was measured at three locations using a thickness gauge. The ultimate tensile strength, Young's modulus, and ultimate strain were obtained from the stress–strain curves ($n = 3$).

Dynamic Mechanical Analysis. Dynamical and mechanical analysis (DMA) of crosslinked mats was carried out on a DMA instrument (Tritec 2000) in torsion mode, heating rate of 2 °C/min and frequency of 1 Hz. The temperature dependence of the storage modulus (G') and loss tangent (tan δ) was plotted in the range of −50 to 150 °C. Crosslink density of the samples was estimated as $v_c = \frac{E'}{RT'}$, where E' is the storage modulus at the onset of the rubbery plateau given by DMA graph, R the gas constant, and T, the absolute temperature at the beginning of the rubbery plateau region.[14]

Cell Morphology Study. To assess the ability of electrospun scaffolds to support cell adhesion and proliferation, mats were seeded with normal human dermal fibroblasts (NHDFs) at a density of 50,000 cell/cm^2. Before cell seeding onto the scaffolds, the rectangular samples (1 cm × 1.5 cm) were sterilized in 70% ethanol for 30 min, washed repetitively in PBS, exposed to UV radiation from both sides, and soaked in complete culture media (RPMI containing 10% fetal bovine serum and 100 U mL^{-1} antibiotics) overnight. The media was then removed and 300 µL of cell suspension gently loaded onto each sample followed by 3 h incubation to allow proper cell attachment. Cell seeded samples were then incubated with sufficient culture media for 1 week. After that, the samples were rinsed twice with PBS to remove non-adherent cells, fixed with 2.5% glutaraldehyde for 1 h, again rinsed in PBS, dehydrated in graded concentrations of ethanol, and finally air dried. The prepared samples were then observed under SEM.

Cell Proliferation Study. Cell compatibility of the crosslinked mats was studied by tetrazolium dye-based colorimetric assay (MTT assay). For the MTT assay, two groups of electrospun mats were selected; GC HEC/PVA1 and PC HEC/PVA1. After sterilization, the samples were incubated with complete media for 24 h and 96 h with an extraction ratio of 6 cm^2 mL^{-1}. At each time point, supernatant media was collected and used as extraction medium with no further dilution.

NHDFs were seeded in 96-well plate at a density of 5000 cells per well and incubated for 24 h. After which, the media was exchanged with prepared extraction medium and left in an incubator for another 24 h. Optical densities (OD) were measured at 570 nm. The cell viability was normalized to that of cells cultured in the culture media without any extracts.

Statistical Analysis

Statistical study of the quantitative data was performed using one-way ANOVA and Tukey's *post hoc* analysis with statistical package software (IBM SPSS Statistical 19.0).

RESULT AND DISCUSSION

Morphology Characterization of Electrospun Scaffold

Figure 1 shows SEM images of electrospun HEC/PVA1 nanofibers and their corresponding structure after chemical and photochemical reactions. SEM micrographs reveal that almost uniform nanofibers with no beads or other irregularities were obtained under the optimized spinning conditions. The average fiber diameters measured from the SEM images for HEC/PVA1 samples (HEC/PVA 36:64) were 486 ± 96 [Figure 1(a)]. The fibers grew thinner as the contribution of the HEC increased (406 ± 53 and 379 ± 82 nm for HEC/PVA2 and HEC/PVA3 respectively, see Supporting Information Figure 1).

It is noticeable that composition of HEC/PVA in the blend influenced fiber diameter as it significantly affects electrospinning solution properties such as viscosity and conductivity.[15] Measuring these values pre-electrospinning process showed that upon increasing the HEC share in PVA/HEC blend solution, viscosity decreased and conductivity increased. For example, while the viscosity value of pure PVA solution was 157 ± 2 cPa, the PVA/HEC with blend ratio of 54:46 had much lower viscosity of 61 ± 3cPa. Similarly the conductivity of pure PVA solution increased from 580 ± 2 µs/cm to 874 ± 2 µs/cm when HEC was blended into PVA solution (PVA/HEC: 54:46). Although HEC inherently is a nonionic polymer, the increase in conductivity can be attributed to its partial ionization in water.

Figure 1(b–e) shows the morphology of electrospun mat with a composition of 36:64 after being crosslinked under chemical and photochemical procedures followed by soaking in PBS for several hours. Crosslinking using GA vapor resulted in complete loss of the fibrous and pore structures resulting in a nonporous flat structure. Considering the presence of enormous water vapor in the crosslink chamber and the high affinity of the scaffolding materials to water, the shape deformation seems reasonable. As crosslinking chamber was saturated with both GA as well as water vapor, the fibers absorbed water vapor more easily and more rapidly than GA vapor. Therefore swelling and fiber merging precedes crosslinking by GA. Immersion of mats in aqueous GA solution also resulted in fused sample which corroborate this fact [Figure 1(c)].

To improve structural preservation, reduced the solubility of the fibers and favored the junction formation through GA crosslinking, crosslinking in propanol/water mixture under acidic condition was used as an alternative method. Since propanol prevents the dissolution of the materials and minimizes the possibility of water absorption and extra swelling of the fibers, fibrous and porous structure of electrospun mats were almost preserved through crosslinking.

Nevertheless, GA crosslinking resulted in an overall increase in fiber diameter. For example, the average fiber diameters of HEC/PVA1, HEC/PVA2, and HEC/PVA3 samples increased to 552 ± 93 nm, 498 ± 61, and 468 ± 83, respectively, which are higher than their original ones. Increase in fiber diameter and stability was more pronounced in samples with higher HEC content. Since GA reacts with hydroxyl groups of HEC and PVA to perform its crosslinking function, the higher HEC content results in higher degree of inter- and intra-fiberal crosslinking

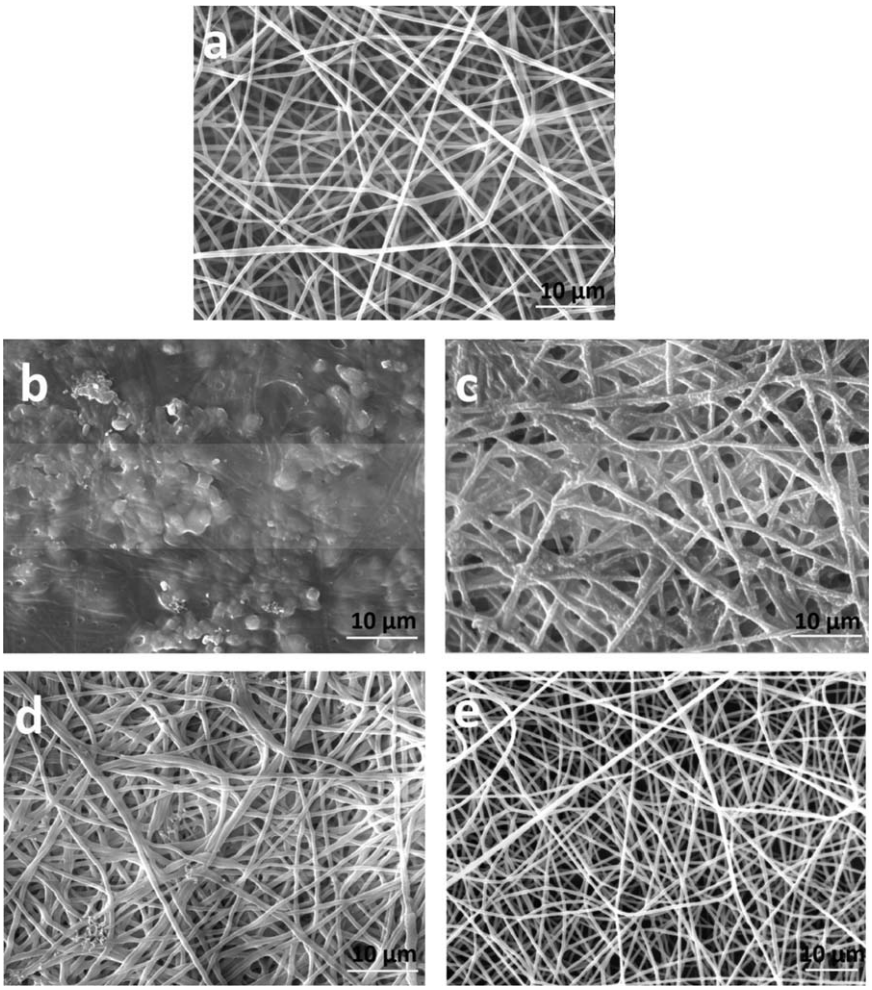

Figure 1. SEM images of (a) as spun, (b) GA vapor crosslinked, (c) GA aqueous solution crosslinked, (d) GA in propanol/water mixture crosslinked, and (e) photocrosslinked HEC/PVA mat (magnification; 4.0k×).

which increase fibers diameters and improves stability.[16,17] Surprisingly, the fiber diameter change after UV crosslinking was not significant ($P > 0.05$). This is probably due to inefficient or low degree of crosslinking.

Morphological changes of the crosslinked mats were further investigated after 3, 7, and 15 days incubation in PBS (pH = 7.4). SEM images of GC HEC/PVA1 and PC HEC/PVA1 mats are presented in Figure 2. GA crosslinked scaffold almost showed no changes in fiber morphology up to 15 days of PBS immersion. Meanwhile, photocrosslinked mat of similar composition changed gradually to a swollen state and lost fibrous morphology after a period of 3 days, and the fibrous structure was fully vanished up to 15 days of PBS submersion. The morphological instability of the photocrosslinked scaffolds along with lack of increase in fiber diameter after crosslinking corroborates ineffective photcrosslinking procedure in mats.

Porosity and Pore Size Determination

Table II represents the scaffold porosity and average pore size for as-spun and crosslinked mats. The porosity was estimated from liquid intrusion and gravimetry methods, and the values appeared to be statistically in good agreement (for various pairwise comparisons $P > 0.05$). It was perceived that as the weight fraction of HEC increased, the porosity of the nonwovens increased, whereas the average pore size decreased. The higher the HEC fraction was, the thinner fibers were deposited. Thinner fibers offered higher porosity, however with smaller pore sizes.[12]

After GA crosslinking, there was no significant difference in the porosity and average pore size of the HEC/PVA mats. Therefore, it can be elucidated that the crosslinking method used here has performed successfully in preserving porous structure of the nonwovens.

On the other hand, there was a remarkable increase in pore size when scaffold underwent photocrosslinking ($P < 0.05$). The increase could have been explained by minimum fiber fusion and degradation of samples during crosslinking.[18]

FTIR Study

The state of crosslinking and the presence of reactive groups in fibers were evaluated by FTIR study. In Figure 3(a), spectra of HEC powder and HEC/PVA fibers before and after crosslinking are shown. FTIR spectra of pure HEC consisted of two principal peaks around 3400 and 2900 cm^{-1} which can be attributed to

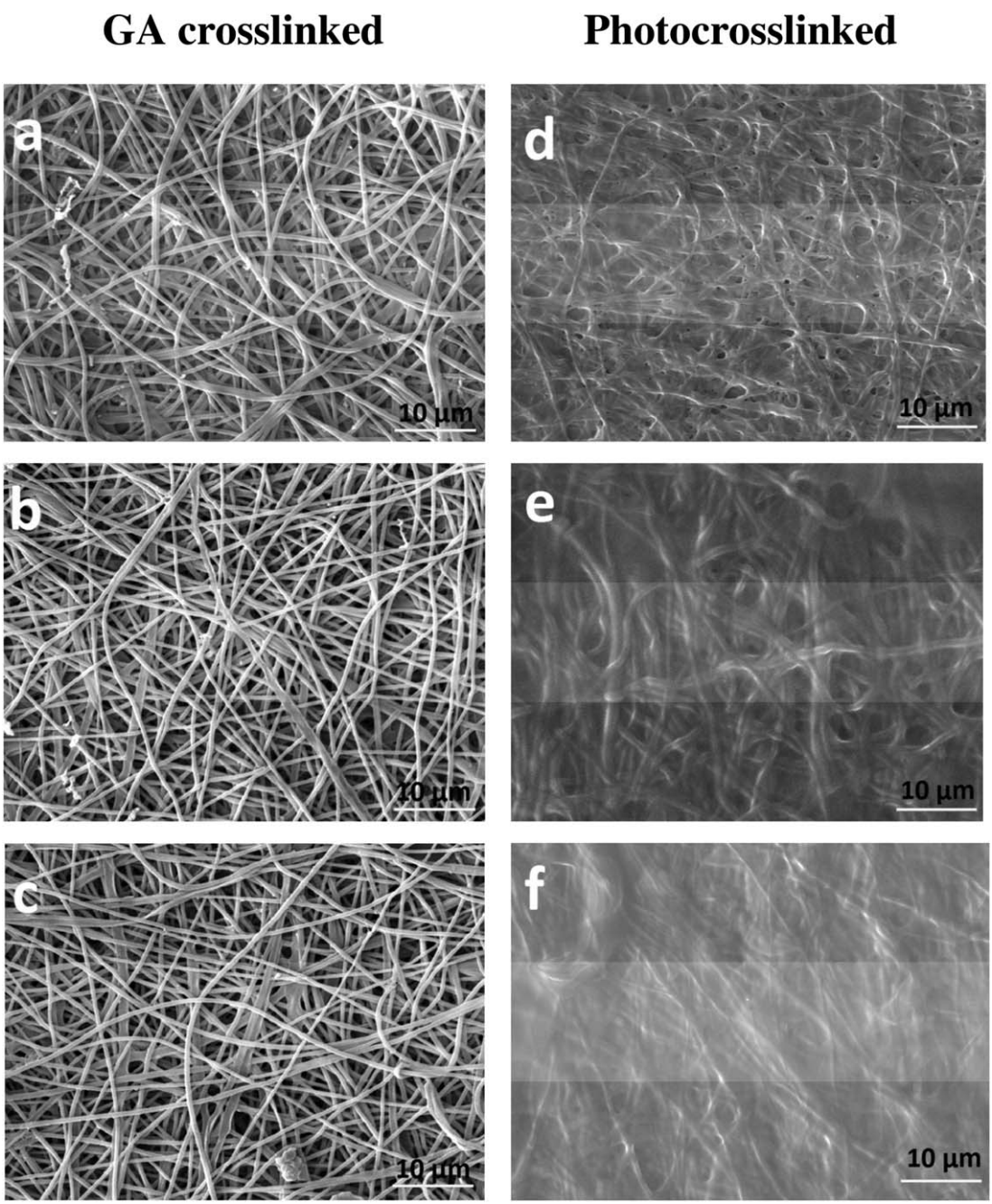

Figure 2. Morphological stability of crosslinked HEC/PVA mat with a composition of 36:64 in PBS for a duration of; (a,d) 3, (b,e) 7, and (c,f) 15 days (magnification; 4.0k×).

characteristic peak of –OH groups and stretching vibration of –CH_2 groups, respectively.[10] As a result of blending, OH band of pure HEC at 3431 cm^{-1} moved to 3382 cm^{-1} in a composition with 36:64 weight ratio. Moving to a lower wave number was indicative of strong intermolecular interactions between the blend's constituents. However, with further HEC blending, the peak was shifted to 3402 and 3425 cm^{-1} for compositions of 45:55 and 54:46, respectively. Following GA crosslinking, peaks' position remained unchanged, while peaks' intensity underwent some changes. As a result of crosslinking, O—H peak intensity was reduced which may denote acetal bridges formation. There was no evidence of GA residual in the samples.

Mechanical Properties of Electrospun Scaffolds

The tensile properties of the electrospun scaffolds with various compositions before and after crosslinking were tested and the results are shown in Table III. The tensile properties of nanofibrous mats are highly dependent on the composition, crystalline, and molecular structure of the fibers, as well as the inter fiber bonding, fiber size and distribution, the porosity, the pore

Table II. Porosity and Average Pore Diameter of as Spun and Crosslinked HEC/PVA Nanofibers

Scaffold code	Porosity % (liquid intrusion)	Porosity % (Gravimetry)	Pore size μm
HEC/PVA1		73 ± 0.3	0.61 ± 0.03
HEC/PVA2		78 ± 1	0.56 ± 0.16
HEC/PVA3		80 ± 1	0.50 ± 0.13
GC HEC/PVA1	66 ± 7	73 ± 9	0.49 ± 0.17
PC HEC/PVA1	84 ± 4	73 ± 7	1.31 ± 0.41
GC HEC/PVA2	79 ± 2	72 ± 4	0.52 ± 0.08
GC HEC/PVA3	83 ± 6	72 ± 4	0.38 ± 0.20

size, and the fiber orientation.[19] By increasing HEC content, ultimate tensile strength and modulus were decreased. This is contrary to our expectation as increasing HEC content in fibers results in smaller fiber diameters which according to literature should have higher tensile strength and modulus.[20] This observation can be justified by several reasons. Simply, synthetic fibers are superior to those produced from natural polymers with respect to mechanical attributes. Moreover, as HEC content increased, the solution spinnability decreased and macroscopic defects appeared along the sample. Moreover, it has been established that increasing the HEC fraction in blended fibers has an adverse effect on the crystalline structure of the said fibers.[7] And finally, suboptimal physical interactions between two components may result in fibers weakening.

As expected, GA crosslinking affected electrospun scaffold tensile characteristics. It improved ultimate tensile strength and elasticity, while decreased ultimate tensile strain. Mechanical strength and increase in modulus as well as ultimate strain reduction after crosslinking is an expected behavior.[4] In fact forming intra- and inter-fiber bonding leads scaffold to be more resistant to deformation. Lower tensile strain after GA crosslinking is also attributable to reduced molecular mobility in the crosslinked polymer network.[4,21]

After photochemical crosslinking, the elastic modulus of the scaffold decreased remarkably ($P < 0.05$), while the ultimate strain of the mat increased substantially ($P < 0.001$). The observed trend for tensile performance contradicts previous reports about photocrosslinked samples.[5,22] Irradiation of polymeric materials always results in both degradation and crosslinking. In our case, the polymer degradation may outperform the crosslinking, thus decreasing mat elasticity. This is corroborated by the fact that in our swelling study in PBS, this sample did not keep its form stability and dissolved in aqueous media. Although crosslinking can improve the tensile strain of polymers,[23] the observed improvement in tensile strain of these samples can be attributed to incomplete fiber fusion during the electrospinning process. Fiber fusion in electrospun mat is known to increases elastic modulus and decrease ultimate strain.[19] In fact, the use of UV lamp inside the electrospinning chamber, elevated chamber temperature, and increased solvent

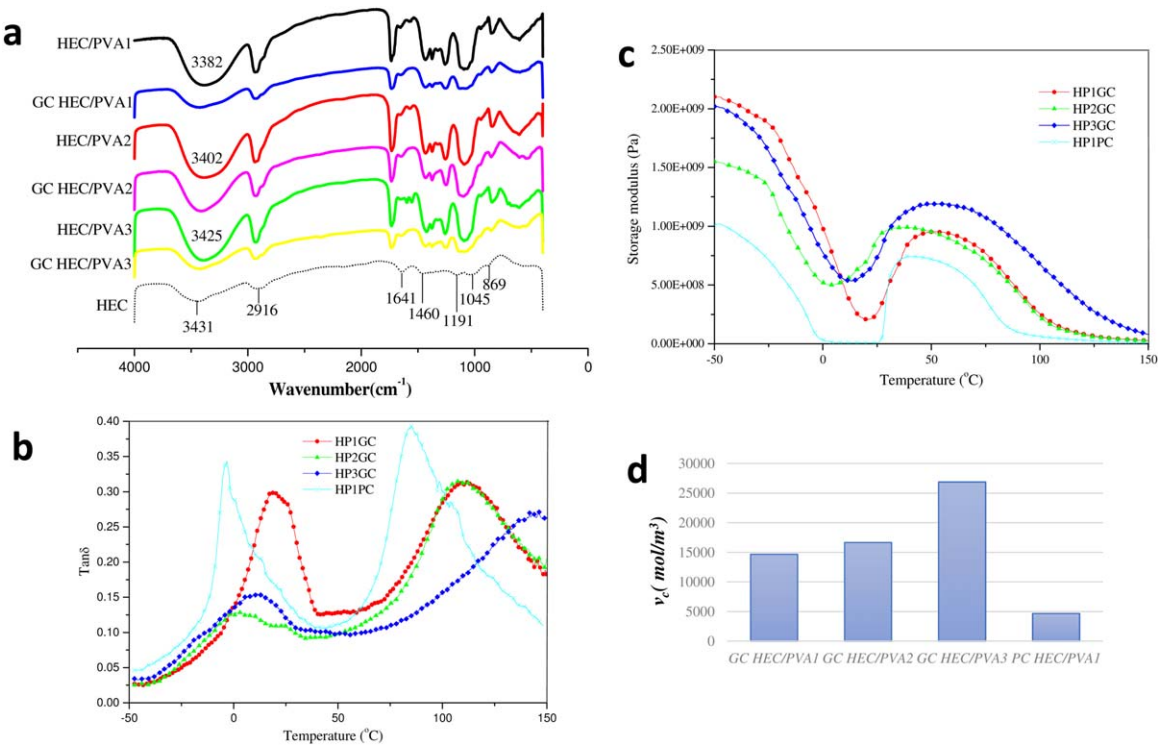

Figure 3. HEC/PVA nanofibers characterization. (a) FTIR spectra of HEC powder, as-spun, and crosslinked nanofibers. (b) Tan δ curves versus temperature of nanofibers. (c) Storage modulus variation of nanofibers versus temperature. (d) Calculated crosslink density of the mats according to rubber elasticity equation. [Color figure can be viewed in the online issue, which is available at wileyonlinelibrary.com.]

Table III. Tensile Properties of As Spun and Crosslinked HEC/PVA Mats of Different Compositions

Sample code	Tensile modulus (MPa)	Ultimate tensile strength(MPa)	Ultimate strain (%)
HEC/PVA1	3.43 ± 0.64	4.64 ± 0.40	10.55 ± 0.69
HEC/PVA2	2.25 ± 0.69	3.29 ±0.34	19.77 ± 0.83
HEC/PVA3	1.83 ± 0.24	2.23 ± 0.30	6.45 ± 0.57
GC HEC/PVA1	4.90 ± 0.76	8.13 ± 0.51	6.60 ± 0.42
PC HEC/PVA1	1.55 ± 0.20	4.76 ± 0.28	19.13 ± 1.85
GC HEC/PVA2	3.58 ± 0.52	6.18 ± 0.17	8.63 ± 1.69
GC HEC/PVA3	3.27 ± 0.23	3.76 ± 0.21	2.92 ± 1.01

evaporation rate can possibly result in electrospun mat with little or no fused fibers.

To provide a better insight into the effect of crosslinking process on structural, thermal, and mechanical properties of the nonwovens mats, DMA was exploited to assess the relaxation behaviors, miscibility, and crosslinking density of fibers. The thermal transition temperature, storage modulus, and calculated crosslink density (ν_c) of the mats studied are also shown in Figure 3(b–d). DMTA curves for each of mats revealed two relaxation temperatures. The first was recognized as β relaxation, related to local motions of HEC and PVA side groups and the second as glass transition of the blended structure. β relaxation was readable in the range of 6–28, −7 to 10, −8 to 25 and −6 to 1.8 °C for GC HEC/PVA1, GC HEC/PVA2, GC HEC/PVA3, and PC HEC/PVA1, respectively. In pure polysaccharide, β relaxation appears at much lower temperature range.[24] However since in HEC, hydroxyl groups are substituted with larger and less movable groups with limited side groups motions, the relaxation shifted to higher temperature. The peak observed at about 100 °C in tan δ curves of the mats could be attributed to glass transition phenomenon of the blended compositions. Having a single T_g is a strong indication of the blended system miscibility.[25] Intermolecular interactions between PVA and HEC due to hydrogen bonding led blend to be homogeneous and endowed with single T_g.

T_g of the PC HEC/PVA1, GC HEC/PVA1, GC HEC/PVA2, and GC HEC/PVA3 mats were found to be at around 85, 105, 105 and 140 °C, respectively. The glass transition of a blended

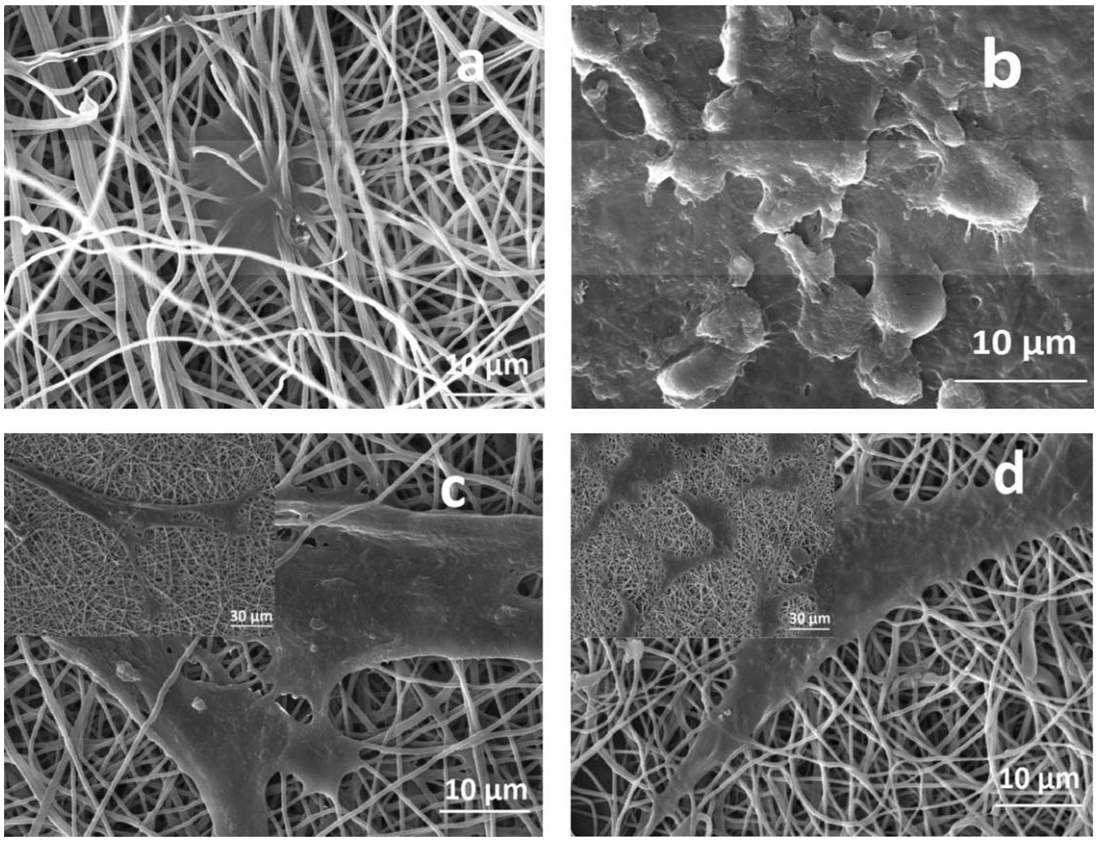

Figure 4. SEM images of dermal fibroblasts adhesion on HEC/PVA nanofibers of different labels; (a) GC HEC/PVA1, (b) PC HEC/PVA1, (c) GC HEC/PVA2, (d) GC HEC/PVA3 mats.

system depends on T_g of the involving materials as well as the proportion of each component. The more HEC content was, the higher T_g was expected. Besides, according to degree of crosslinking values, 54% HEC loaded mat revealed the highest degree of crosslinking, thus the stiffest structure. Moreover, increasing the blend ratio of HEC to 54% may impede the polymeric chain mobility. Structural stiffening as well as the reduced chain mobility affected the T_g synergistically, both of which tended to increase it.

According to the calculated values, crosslink density decreased once HEC content increased. Moreover, the value was lower for photocrosslinked sample comparing GA crosslinked one of similar composition. Tan δ variations versus temperature further confirmed the crosslinking results. As a general trend, increasing HEC content decreased tan δ value, hence viscose properties. The higher HEC was, the more effectively crosslinking acted which gave rise to elastic properties enchantment.

Cell Morphology and Proliferation Study

SEM images of the human dermal fibroblasts after 7 days of culture on the fibrous mats are displayed in Figure 4(a–d). SEM micrographs confirmed that nanofibrous mats were able to induce appropriate level of cell adhesion, spreading, and morphology. The cells appeared to be more speared and aligned as HEC content increased. This is most likely due to reduction in fiber diameter. Surface coating and pore bridging onto GC HEC/PVA3 mat indicated the proper activity and ECM secretion of the resident cells over the said mat.[26] It is well established that thinner fibers afford more surface areas to absorb reactive proteins from the culture medium, thus presenting more binding sites to cell membrane receptors.[15] In case of photocrosslinked mat, as it was seen in Figure 4(b), the fibrous morphology of the mat was lost after a period of 3 days. Therefore the observed reduction in cell spreading and alignment compared to other samples seems reasonable.

Interestingly, there is some evidence of cell infiltration in a mat with 36% weight fraction of HEC (GC HEC/PVA1) as can be seen in Figure 4(a). Although this mat had the highest value of porosity and pore diameter compared to GC HEC/PVA2 and GC HEC/PVA3, however; the pore size was by far smaller than targeted value for fibroblast cell penetration (at least 10–15 μm). Crosslink density of the GC HEC/PVA1 was lower compared to GC HEC/PVA2 and GC HEC/PVA3, which may cause more material leach from the mat after being soaked in media for a period of 7 days and create more open spaces for cell ingress. The cell viability of GC HEC/PVA1 and PC HEC/PVA1 samples were further evaluated using MTT assay.

Results revealed cell viability in the range of 71–84% suggesting both methods of the crosslinking resulted in mat with no toxicity for cells. In case of GA crosslinked samples, there was no significant difference in cell viability after contact with extract for a period of 96 h compared with 24 h. This may confirm that there was no or little amount of GA traces in the structure that imparted any *in vitro* toxicity. In photocrosslinked sample, however; cell viability reduced significantly after 96-h incubation with extraction medium as compared to 24 h. Less crosslinking density and more hydrophilic nature of the photocrosslinked mat may lead polymeric constituents liberate to the cell culture medium, thus impairing cell viability. Although cell viability value diminished after 96 h, it still lies well within the acceptable range for cell survival.

CONCLUSIONS

Change of electrospun nanofibers following crosslinking procedure is imminent phenomenon. The properties of as-spun fibers are largely different with those of crosslinked mats. So having an understanding of the crosslinking process on mat features is necessary. Present study was carried out to detect the influence of chemical and photochemical crosslinking on HEC-based nanofibers. From the results, it can be concluded that both procedures impacted morphology, tensile behavior, porosity, thermal properties, and biocompatibility of the nanofibers. Chemical crosslinking outperformed photochemical approach in the case of long-term morphology preservation and cell interaction. Chemically crosslinked HEC-based nanofibers seem very promising to induce appropriate skin cells adhesion and function. Further modifications like addition of chemical or biological cell friendly moieties to fibers or application of different surface treatment processes will lead these fibers to be very promising for skin tissue restoration.

ACKNOWLEDGMENTS

The authors would like to express their sincere gratitude to Iran National Science Foundation (Grant No. 90004627) for supporting this research.

REFERENCES

1. Lee, K. Y.; Jeong, L.; Kang, Y. O.; Lee, S. J.; Park, W. H. *Adv. Drug Deliv. Rev.* **2009**, *61*, 1020.
2. Khorshidi, S.; Solouk, A.; Mirzadeh, H.; Mazinani, S.; Lagaron, J. M.; Sharifi, S.; Ramakrishna, R. J. *Tissue Eng. Regen. Med.*, **2015**. DOI: 10.1002/term.1978.
3. Reddy, N.; Reddy, R.; Jiang, Q. *Trends Biotechnol.* **2015**, *33*, 362.
4. Naseri, N.; Algan, C.; Jacobs, V.; John, M.; Oksman, K.; Mathew, A. P. *Carbohydr. Polym.* **2014**, *109*, 7.
5. Xu, X.; Zhang, J. F.; Fan, Y. *Biomacromolecules* **2010**, *11*, 2283.
6. Xu, X.; Zhang, J. F. *Curr. Tissue Eng.* **2012**, *1*, 2.
7. Zulkifli, F. H.; Hussain, F. S. J.; Rasad, M. S. B. A.; Mohd Yusoff, M. *Carbohydr. Polym.* **2014**, *114*, 238.
8. Zulkifli, F. H.; Jahir Hussain, F. S.; Abdull Rasad, M. S. B.; Mohd Yusoff, M. *Polym. Degrad. Stabil.* **2014**, *110*, 473.
9. Gunn, J.; Zhang, M. *Trends Biotechnol.* **2010**, *28*, 189.
10. Zhang, H.; Nie, H.; Li, S.; White, C. J. B.; Zhu, L. *Mater. Lett.* **2009**, *63*, 1199.
11. Rošic, R.; Kocbek, P.; Baumgartner, S.; Kristl, J. *J. Drug Deliv. Sci. Technol.* **2011**, *21*, 229.

12. Soliman, S.; Pagliari, S.; Rinaldi, A.; Forte, G.; Fiaccavento, R.; Pagliari, F.; Franzese, Minieri, M.; Di Nardo, P.; Licoccia, S.; Traversa, E. *Acta Biomater.* **2010**, *6*, 1227.
13. Loh, Q. L.; Choong, C. *Tissue Eng.* **2013**, *19*, 485.
14. Treloar, L. R. G. The Physics of Rubber Elasticity; Oxford University Press: London, **2009**.
15. Agarwal, S.; Wendorff, J. H.; Greiner, A. *Adv. Mater.* **2009**, *21*, 3343.
16. Rojas, J.; Azevedo, E. *Int. J. Pharm. Sci. Rev. Res.* **2011**, *8*, 28.
17. Destaye, A. G.; Lin, C. K.; Lee, C. K. *Appl. Mater. Interfaces* **2013**, *5*, 4745.
18. Wach, R.; Mitomo, H.; Nagasawa, N.; Yoshii, F. *Nucl. Instrum. Methods Phys. Res. Sect. B* **2003**, *211*, 533.
19. Baji, A.; Mai, Y. W.; Wong, S. C.; Abtahi, M.; Chen, P. *Compos. Sci. Technol.* **2010**, *70*, 703
20. Wong, S. C.; Baji, A.; Leng, S. *Polymer* **2008**, *49*, 4713.
21. Panzavolta, S.; Gioffre, M.; Focarete, M. L.; Gualandi, C.; Foroni, L.; Bigi, A. *Acta Biomater.* **2011**, *7*, 1702.
22. Ifkovits, J. L.; Devlin, J. J.; Eng, G.; Martens, T. P.; Vunjak-Novakovic, G.; Burdick, J. A. *ACS Appl. Mater. Interfaces* **2009**, *1*, 1878.
23. Sharifi, S.; Grijpma, D. W. *Macromol Biosci.* **2012**, *12*, 1423.
24. Lee, Y. M.; Kim, S. H.; Kim, S. J. *Polymer* **1996**, *37*, 5897.
25. Santos, C.; Silva, C. J.; Buttel, Z.; Guimaraes. R; Pereira, S. B.; Tamagnini, P.; Zile, A. *Carbohydr Polym* **2014**, *99*, 584.
26. Lowery, J. L.; Datta, N.; Rutledge, G. C. *Biomaterials* **2010**, *31*, 491.